IEEE Access
Multidisciplinary ⋮ Rapid Review ⋮ Open Access Journal

Received 19 July 2023, accepted 3 August 2023, date of publication 7 August 2023, date of current version 15 August 2023.

Digital Object Identifier 10.1109/ACCESS.2023.3302772

RESEARCH ARTICLE

High-Speed MW-Class Generator With Multi-Lane Slotless Winding for Hybrid-Electric Aircraft

EIRIK KVÅLE MIKKELSEN[1], ALEXEY MATVEEV[1,2], AND JONAS KRISTIANSEN NØLAND[1], (Senior Member, IEEE)

[1]Department of Electric Energy, Norwegian University of Science and Technology (NTNU), 7034 Trondheim, Norway
[2]Alva Industries AS, 7038 Trondheim, Norway

Corresponding author: Jonas Kristiansen Nøland (jonas.k.noland@ntnu.no)

ABSTRACT This paper presents a comprehensive design and analysis of a high-speed, multi-lane, 2.5 MW, 15 000 rpm, 3 kV slotless generator system tailored for hybrid-electric aircraft. The armature of this generator incorporates FiberPrinting^{TM} technology, featuring four galvanically isolated concentric winding rings. An assessment of the generator's performance metrics was conducted through finite element analysis (FEA). The 2.5 MW slotless 8-pole generator achieved a power density of 24.4 kW/kg (for active mass) and an efficiency above 99 % at the current density of 15 A/mm^2. To further enhance the system's efficiency, we investigated the possibility of incorporating a filter between the generator and frequency converter. However, this investigation revealed that the weight and losses associated with the filter outweigh any potential gains in generator efficiency. Additionally, the study explored the impact of elevating the current density to levels comparable to the state-of-the-art (SotA) machines (20-27.5 A/mm^2). The results indicate that such an enhancement would significantly raise the power density to 35-40 kW/kg. Furthermore, increasing the number of poles from 8 to 12, in combination with the elevated current density, can surpass the threshold of 40 kW/kg. Comparing our findings against the SotA, we demonstrate that the proposed topology exhibits the potential to outperform conventional technologies, provided adequate cooling measures are implemented.

INDEX TERMS Generator, hybrid-electric aircraft, slotless machines, fault-tolerant drive systems.

NOMENCLATURE

α_p	Pole pitch, $[mm]$.
δ, l_m, h_{enc}, h_s	Air gap, magnet, magnet sleeve, and winding height, $[mm]$.
η, η_n	Efficiency and rated efficiency, $[\%]$.
Γ_e	Electrical torque, $[Nm]$.
μ_r	Relative permeability of magnets, $[-]$.
ρ_{air}, ρ_{cu}, ρ_{ins}	Air, copper, and insulation mass density, $[kg/m^3]$.
ρ_{enc}, ρ_{pm}, ρ_{fe}	Magnet enclosure, magnet, and steel mass density, $[kg/m^3]$.
ρ	Mass density, $[kg/m^3]$.
σ_{pm}, σ_{cu}	Magnet and copper conductivity, $[S/m]$.
ϱ_a, ϱ_{tot}	Active mass and total mass power density, $[kW/kg]$.
τ_a, τ_{tot}	Active mass and total mass torque density, $[kW/kg]$.
ξ	Ratio between AC and DC resistance.
a_s, a_c, a_w	Slot, coil, and wire area, $[mm^2]$ or $[m^2]$.
B_r, B_y	Magnet's remanent flux density and stator yoke flux density, $[T]$.
C_w	Rotor skin friction coefficient, $[-]$.
D_r, D_s	Outer rotor and stator diameter, $[mm]$.
dS	Surface integral operator, $[m^2]$.
f, f_{sw}	Fundamental frequency and inverter switching frequency, $[Hz]$ or $[kHz]$.
m_{fe}, m_{enc}, m_{pm}	Stator yoke, rotor enclosure, and magnet mass, $[kg]$.
I_{ph}	Phase current (rms), $[A]$.
J_s, J_{pm}	Stator and magnet current density, $[A/mm^2]$ or $[A/m^2]$.
k_{fill}	Winding filling factor, $[-]$ or $[\%]$.

The associate editor coordinating the review of this manuscript and approving it for publication was Rosario Pecora.

l_a, l_{ew}	Active machine length and end-winding length, $[m]$ or $[mm]$.
L_d, L_q, L_{ph}	Direct-axis, quadrature-axis, and total phase inductance, $[H]$ or $[pu]$.
m_{cu}, m_{ew}, m_{ins}	Copper, end-winding, and insulation mass, $[kg]$.
m_{tot}, m_a	Total and active machine mass, $[kg]$.
n_s	Nominal rotational speed, $[rpm]$.
N_s, N_{ph}, N_t	Number of stator segments, number of stator phases per segment and number of turns per slot in each segment.
P_e, P_m	Generator and motor power, $[MW]$.
P_{pm}, P_w	Magnet and windage losses, $[kW]$.
p, q	Number of poles, and number of slots per pole and phase.
R_{dc}, R_{ph}	Coil DC resistance and phase resistance, $[\Omega]$.
T_e	Electrical time period, $[ms]$ or $[s]$.
U_{dc}, U_l, E_l	DC-link voltage, and AC fundamental load and no-load line voltage (rms), $[V]$.
w, b	Wingspan and aircraft length, $[m]$.
h_y, h_s	Stator yoke thickness and armature ring height, $[mm]$ or $[m]$.
P_{loss}, P_{cu}, P_{fe}	Total losses, copper losses, and steel losses, $[kW]$.

I. INTRODUCTION

Over the last decade, significant advancements have been made in the development of hybrid-electric aircraft (see example in Fig. 1). While the realization of large all-electric aviation still faces challenges related to energy storage, it is expected that large-scale hybrid-electric aircraft concepts will be feasible by the 2030s [1]. Various companies, such as Honeywell (see Fig. 2), have introduced turbo-generator solutions in response to this emerging trend. It is projected that the anticipated increase in battery-specific energy density from the 2030s and 2040s will enable regional hybrid-electric aircraft to meet up to 75 % of market demand [2]. Therefore, the efficient and power-dense design of electrical machines and generators is crucial for the success of hybrid-electric propulsion systems. Golovanov et al. emphasized the necessity of achieving power densities of approximately 20 kW/kg for multi-MW propulsion systems [3]. Consequently, the demand for generators capable of operating at high rotational speeds, around 15 000 rpm or even higher, is incentivized within the context of hybrid-electric aviation [3], [4], [5], [6]. Typically, hybrid-electric concepts involve generators in the power range of 0.5 MW to 4 MW, operating at voltage levels of 2 kV to 3 kV.

One of the potential avenues for weight reduction involves the utilization of machines with a high number of poles to minimize the thickness of the stator and rotor yokes [7]. However, the combination of high rotational speeds and a large number of poles results in a high fundamental electrical frequency. To optimize performance under these conditions,

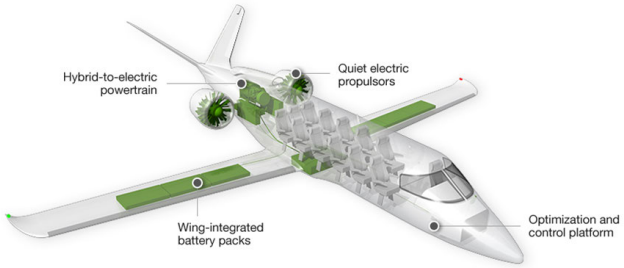

FIGURE 1. Example of hybrid electric aircraft by Zunum Aero.

the adoption of a slotless topology can mitigate core losses and reduce system mass by eliminating teeth in the stator [8], [9]. Previous studies have demonstrated the potential of slotless topologies in high-speed operations, achieving comparable or even superior performance compared to slotted topologies [10], [11]. An additional advantage of the slotless topology is the absence of cogging torque and low torque ripple [8], [12]. For instance, Yoon et al. successfully developed a 1 MW slotless motor with a power density of 14 kW/kg and an efficiency ranging from 97.2 % to 98.3 % [7], [13].

Matveev has introduced a modular converter topology that can be connected in series or parallel to a multi-lane electrical machine [14]. The concept of modularity holds great promise for permanent magnet machines in electric aviation, offering advantages such as high power density, efficiency, and fault tolerance. [15].

In this paper, we aim to combine the benefits of a slotless stator design with the concept of modularity to exploit the advantages of low weight and enhanced redundancy and reliability [16]. Furthermore, we will analyze the hybrid-electric powertrain and examine how it influences the design considerations for the slotless generator under investigation. This comprehensive approach will provide a broader analysis of the generator and its interaction with the hybrid-electric propulsion system, surpassing the scope of existing studies.

The remainder of this paper is structured as follows: Section II presents a qualitative description of the slotless stator topology considered in this study. In Section III, we outline the methodology and assumptions employed, while also providing specifications for the case study of the hybrid-electric aircraft. The main findings and results are then presented in Section IV. Finally, Section V concludes the paper, summarizing the key insights and discussing avenues for future research.

II. SLOTLESS TECHNOLOGY DESCRIPTION

The slotless generator in this study utilizes a unique winding technology known as FiberPrinting^{TM} [17]. This choice of technology significantly enhances the performance of the generator, benefiting from high copper fill factor. The stator rings in this generator are FiberPrinted using thin Litz wire, which is then molded.

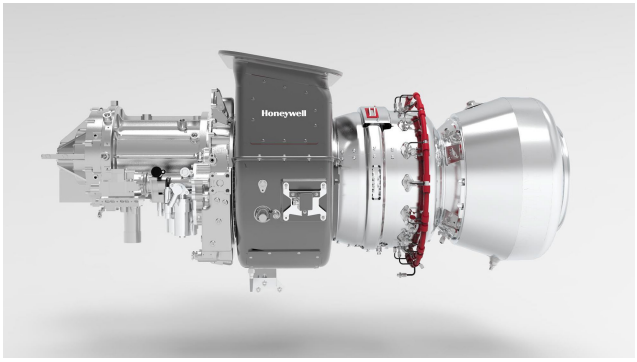

FIGURE 2. Turbogenerator by Honeywell.

A. SCALABLE SOLUTION

A machine called the FiberPrinter, partially resembling weaving machines from the textile industry, intertwines litz wires with the carrying fiber in an automatic process to produce a copper mat with four main attributes: length, width, thickness, and pole number, as seen in Figs. 3 and 4. Since the copper mat is rolled up and potted as a cylinder, the length of the mat determines the diameter of the resulting stator. The width of the mat, therefore, determines the axial length of the stator. The thickness and pole-number of the copper mat are tuned in conjunction to achieve the desired machine characteristics for the use case.

The simplicity of electrical machines made by FiberPrinting^{TM} is that they have perfectly cylindrical stators with only a few design parameters. Such stators can be scaled to any size, as seen in Fig. 5.

Rotors of slotless machines use surface-mounted permanent magnets in either a radial array or Halbach array configuration [18]. The rotors are assembled with proprietary equipment and processes.

B. NO SATURATION

Design of an iron-cored machine is always taking into account saturation of the iron teeth. The current-torque relationship for a slotless machine is linear up to much higher currents than for iron-cored motors, enabling higher torque and power output.

C. LOWER IRON LOSSES

Losses in the teeth of iron-cored machines make a considerable part of the total losses, reducing machine efficiency. In slotless machine, iron losses take place only in the back iron, which is usually made of thin laminations and is not heavily loaded magnetically, making the losses very low compared to the copper losses.

D. REDUCED NOISE AND VIBRATION

Iron-cored generators often have a high amount of torque ripple due to the asymmetric interaction between the magnetic rotor and the iron teeth of the stator. The high level of torque ripple causes a high level of audible noise due to the induced mechanical vibrations. A slotless machine has virtually zero torque ripple due to the symmetrical magnetic interaction between the stator and the rotor. A symmetrical magnetic interaction is achieved since the laminations around the stator are perfectly cylindrical. The absence of torque ripple reduces the vibrations and the audible noise.

TABLE 1. Key specifications of the power ratings and the spatial extent of the hybrid-electric powertrain.

P_e	P_m	b	w
2.5 MW	2.0 MW	28.6 m	26.2 m

E. LOW SENSITIVITY TO LARGE AIR GAPS

Iron-cored machines require as small magnetic air gaps as possible to be compact. The high-speed machines have to use retention screen on the rotor which increases the magnetic air gap and makes the iron-cored machines considerably less compact. Slotless machines inherently have large magnetic air gaps as the slotless winding has magnetic permeability equal the magnetic permeability of air. This feature make slotless almost non-sensitive to the presence of the retention screen on the rotor.

F. REDUNDANT SOLUTION

To meet the requirements for flight safety, there was developed a redundant solution with several concentric windings based on slotless PM technology (Fig. 6). This solution allows for maintaining a fully symmetrical pattern of the magnetic field around the circumference of the stator and rotor even when one of the power electronics converters or one of the stator windings is faulted, thus maintaining vibration-free operation. It is worth noting that two and two non-neighboring segments are paired to form a DC link through the combination of inverters.

III. METHODOLOGY AND ASSUMPTIONS

This section presents the case study and the assumptions made in this research. Fig. 7 shows a generic sketch of a regional hybrid-electric aircraft that will be considered in this paper, and Fig. 8 shows the multi-lane topology. The generator, together with a gas turbine, is placed in the fuselage to generate the electrical power fed to the electric distribution system in the middle of the airplane, including one electric propulsion motor as the main load. Key parameters of the aircraft are provided in Table 1.

A. CASE STUDY

The main focus will be placed on the slotless generator in relation to the hybrid-electric propulsion system. An initial geometric design from an analytical design procedure where implemented in the FEA environment. After the initial design was implemented, parametric sweeps on the rotor radius and magnet length were run to find the most power-dense design,

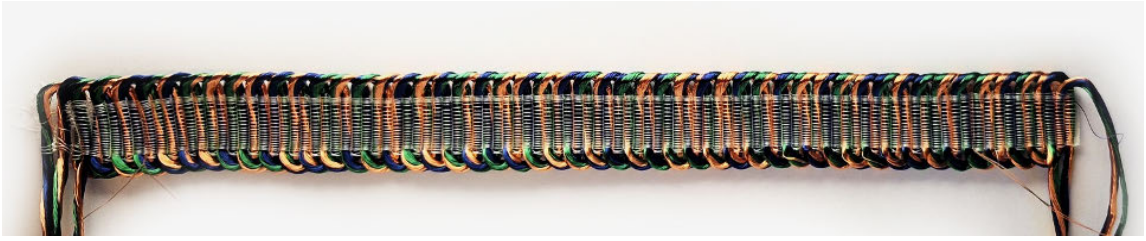

FIGURE 3. Example of a copper mat produced using FiberPrinting™.

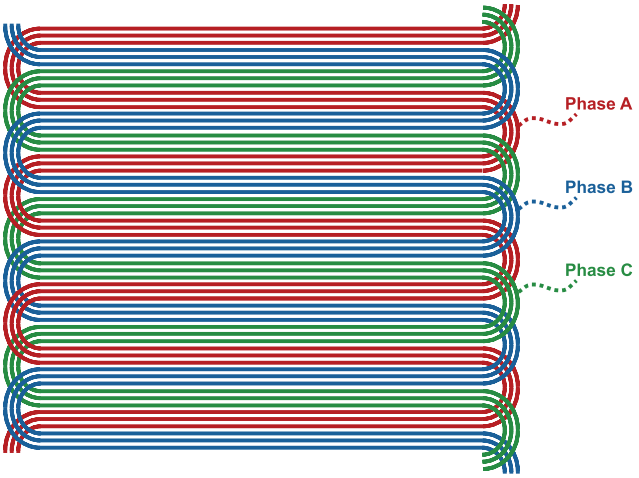

FIGURE 4. The winding diagram for each stator mat including end-winding. Number of turns (N_t) per slot is 3.

FIGURE 5. Examples of FiberPrinted stators in different sizes.

TABLE 2. Magnetic design constraints.

B_r	μ_r	l_m	B_y
1.4 T	1.05	$\leq$ 35 mm	$\leq$ 1.7 T

according to the magnet and electric design requirements listed in Tables 2 and 3. Fig. 9 illustrates a 2-D one-pole cross-section of the generator, and Fig. 10 the axial cross-section of the generator. The maximum flux density in the yoke was set to a value of 1.7 T, and the magnetic properties of the yoke are presented by a BH-curve in Fig. 11. The geometric properties of the final optimized 3 kV generator are listed in Table 4.

B. MASS ESTIMATION

The generator's mass is found by applying the surface integral over the one-pole geometry in the FEA environment (see Fig. 9). The surface integral in eq. (1) is performed over each geometric domain of the one-pole geometry.

$$m_{tot} = \rho p l_a \iint_S dS \tag{1}$$

It is worth noting that the one-pole FEA model of the generator does not include a specific geometric domains for the insulation, as seen in Fig. 9. Nevertheless, the fill factor of the windings can be implicitly included in the mass estimation, according to eqs. (2) and (3).

$$m_{cu} = \rho_{cu} p k_{fill} l_a \iint_{windings} dS \tag{2}$$

$$m_{ins} = \rho_{ins} p (1 - k_{fill}) l_a \iint_{windings} dS \tag{3}$$

The material mass densities are listed in Table 5.

1) END-WINDING MASS

Since the generator model is 2-D, eq. (1) can not be applied to estimate the end-winding mass. Assuming the end-winding has the shape of a half-circle equal to the generator's pole pitch, the length of one end-winding piece and the total end-winding mass are given by eqs. (4) and (5). Fig. 12 shows a three-dimensional (3)-D) of the end-windings.

$$l_{ew} = \frac{1}{2} \pi \alpha_p \tag{4}$$

$$m_{ew} = 2 \rho_{cu} p N_t N_{ph} N_s \alpha_p a_w \tag{5}$$

C. LOSS EVALUATION

1) MAGNET LOSSES

The magnet losses are calculated using a surface integral with eq. (6) over the magnet area in FEA environment [19].

$$P_{pm} = \frac{1}{T_e} \int_0^{T_e} \left(\iint_{magnets} l_a \frac{J_{pm}(t)^2}{\sigma_{pm}} dS \right) dt \tag{6}$$

These losses are negligible in comparison to the copper and steel losses. Since the generator has a slotless topology, there

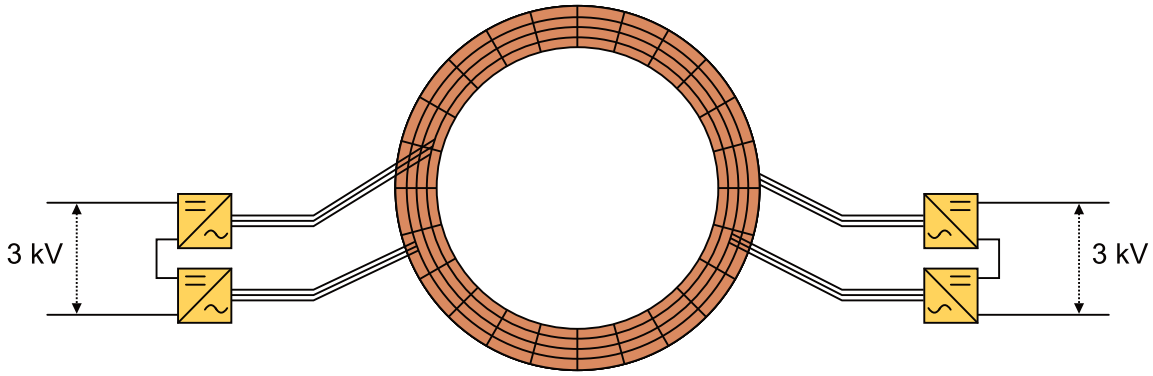

FIGURE 6. Layout of the modularity concept with four concentric stator rings described in patent NO345844B1 (one of the realization variants) [14].

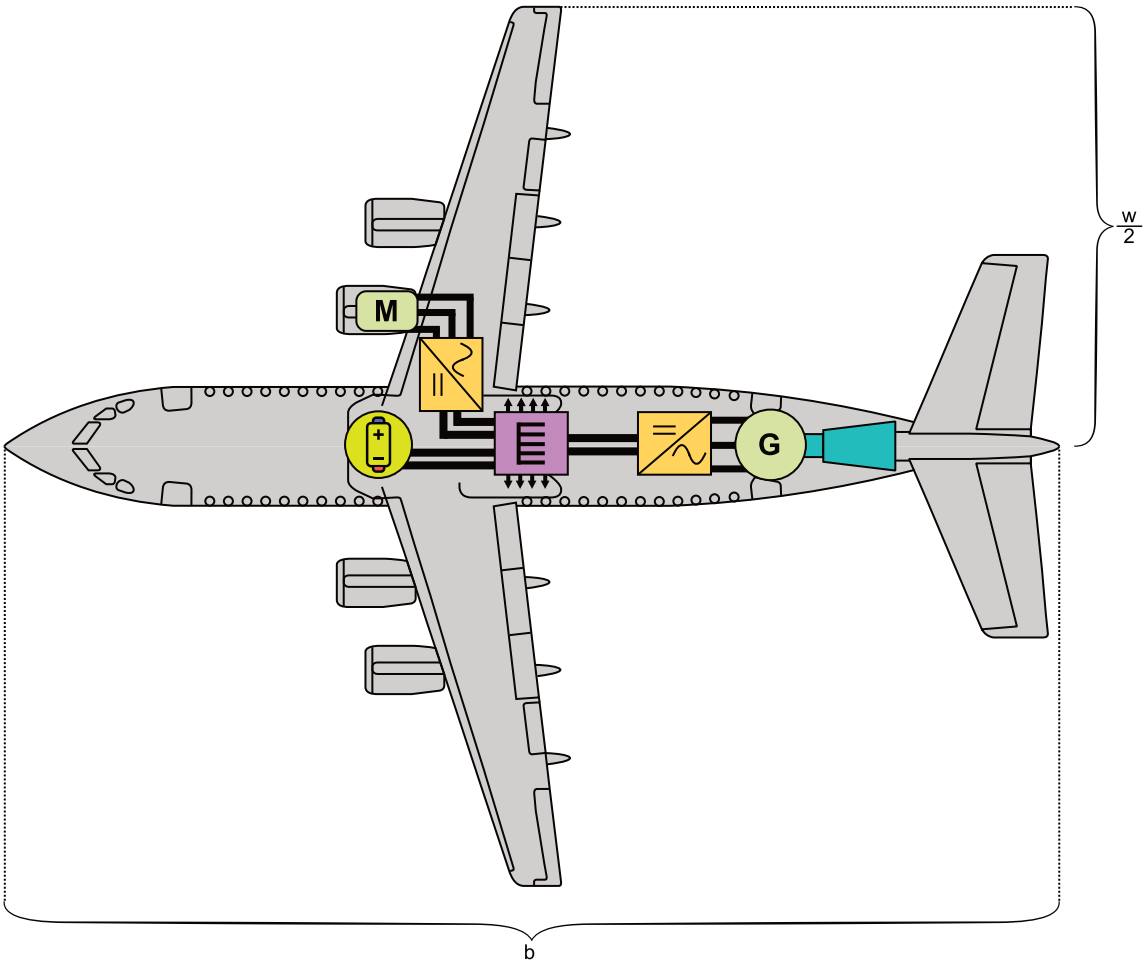

FIGURE 7. Hybrid-electric propulsion powertrain onboard a regional aircraft, including a 2.5-MW generator (G) fed by an onboard gas turbine, inverters, power distribution, onboard battery storage, and a 2.0-MW electric motor (M).

TABLE 3. Electrical design requirements and limitations.

P_e	n_s	f	U_l	I_{ph}	J_s	p	q	N_s	N_{ph}	N_t	k_{fill}	h_s
2.5 MW	15 000 rpm	1000 Hz	1100 V	328 A	$\leq$ 15 A/mm^2	8	1	4	3	3	35 %	$\geq$ 4 mm

are no slots causing harmonics in the air gap. With little air gap harmonics, the magnet losses will be negligible due to low eddy currents in the magnets. However, the magnet losses will increase after introducing the current harmonics from

TABLE 4. Optimized geometric properties of the 2.5-MW, 3-kV, 15000-rpm slotless FiberPrinted generator.

D_r	D_s	l_a	l_m	δ	h_{enc}	h_s	h_y	a_s	a_c	a_w
275.0 mm	356.2 mm	238.0 mm	32.5 mm	3.0 mm	2.0 mm	4.9 mm	16.0 mm	187.25 mm^2	87.37 mm^2	21.84 mm^2

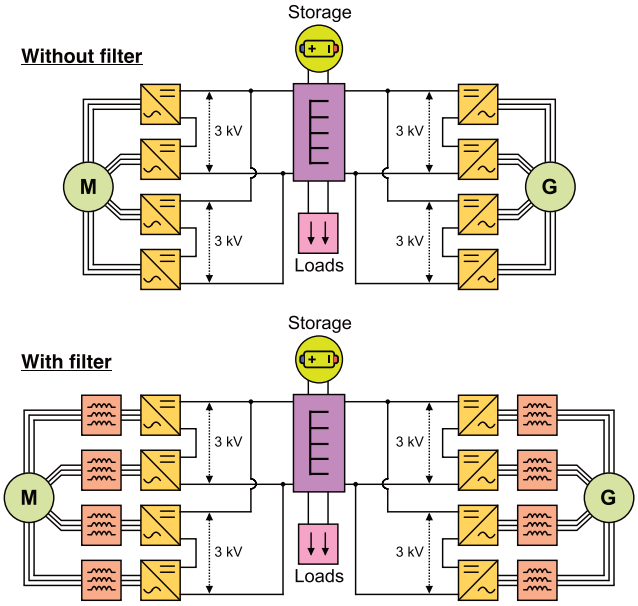

FIGURE 8. Schematic diagram of hybrid-electric multi-lane powertrain with and without filter.

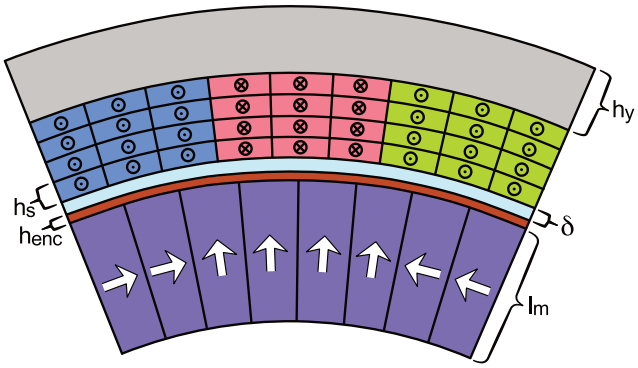

FIGURE 9. Two-dimensional (2)-D) radial cross-section of one pole pitch of the generator with 4 concentric armature segments (N_s), 3 phases per armature (m), and 3 turns per slot in each segment (N_t). The rotor Halbach array has 8 tangential segments per pole. Geometry is used for 2-D FEA modeling with magnetic insulation at inner and outer diameter, and anti-periodic boundary conditions at side boundaries.

TABLE 5. Mass densities of materials in different domains.

ρ_{cu}	ρ_{ins}	ρ_{enc}	ρ_{pm}	ρ_{fe}
8490 kg/m^3	1300 kg/m^3	1750 kg/m^3	7600 kg/m^3	7490 kg/m^3

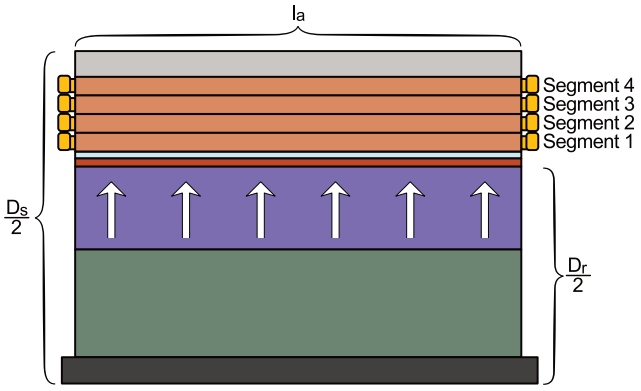

FIGURE 10. Two-dimensional (2)-D) axial cross-section of the generator. The four different stator segments are indicated.

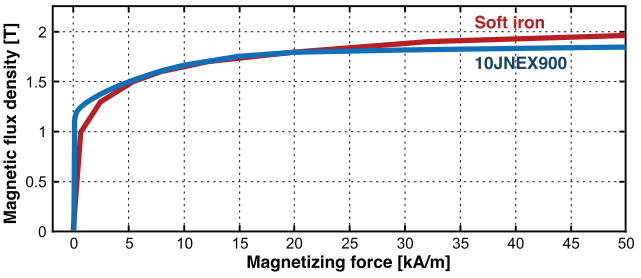

FIGURE 11. Nonlinear B-H curve of conventional soft iron compared to the silicon steel 10JNEX900 designed for high-frequency operation with lamination thickness of 0.1 mm and a stacking factor of 97 %.

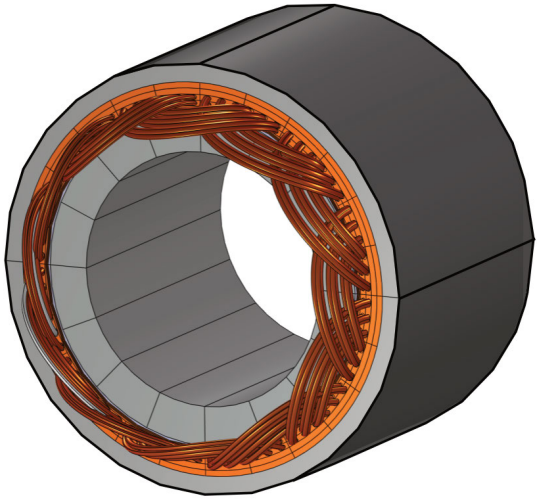

FIGURE 12. Three-dimensional (3)-D) end-windings depicted on stator ring number 1 and 2.

the power inverter feeding the generator. Nevertheless, with a significant increase in magnet losses, there will be a rotor overheating risk.

Magnet segmentation is a way of decreasing magnet losses. The eddy currents' amplitude can be reduced by dividing the magnet into several segments. For example, in [20], the magnet losses in a Halbach array were reduced by 80 % when

TABLE 6. Fitting coefficients for steel 10JNEX900.

Coefficient	Value
k_{h0}	0.01776
k_{h1}	−0.2435
k_{h2}	0.02321
k_{h3}	−0.00542
k_{e0}	$8.200 \cdot 10^{-6}$
k_{e1}	$2.023 \cdot 10^{-5}$
k_{e2}	$-3.292 \cdot 10^{-5}$
k_{e3}	$1.210 \cdot 10^{-5}$

The goodness of fit R^2 was 99.99 % with a sum of squared estimate of errors (SSE) equal to 0.0701.

dividing the magnets into axial segments. Since the model in this paper is a 2-D model, the magnet will be split tangentially into 1, 2, and 4 tangential segments, respectively.

2) STEEL LOSSES

The steel losses were calculated by implementing the CAL2 method in the FEA environment [21]. The curve fitting tool in Matlab was used to fit the coefficients in eq. (7) with the loss data of the electrical steels. The loss data for 200 Hz, 400 Hz, and 1000 Hz was included to include the frequency dependency.

$$\frac{P_{fe}}{m_{fe}} = k_h(f, \hat{B}) f B^2 + k_e(f, \hat{B}) f^2 B^2 \tag{7}$$

A third-order polynomial was chosen as it provided a sufficient fit with the loss data (values given in Table 6).

$$k_e = k_{e0} + k_{e1} B + k_{e2} B^2 + k_{e3} B^3 \tag{8}$$

$$k_h = k_{h0} + k_{h1} B + k_{h2} B^2 + k_{h3} B^3 \tag{9}$$

3) AC AND DC COPPER LOSSES

The copper losses were found by implementing eqs. (10) and (11) in the FEA environment. As the conductivity is temperature-dependent, the DC losses were evaluated at temperatures ranging from 20 to 220 °C. The coefficient ξ was applied to account for the difference between AC and DC copper loss [22], [23].

$$P_{cu} = N_s N_{ph} I_{ph}^2 \underbrace{\xi R_{dc}}_{R_{ph}} \tag{10}$$

$$R_{dc} = \int \frac{N_t l_a}{\sigma_{cu} a_c S} dS \tag{11}$$

4) WINDAGE LOSSES

The high rotational speeds required in the electric aviation industry generates significant mechanical losses due to the frictional forces. Viscous frictional forces occur between the moving rotor and the confined air within the air gap [24].

$$P_w = C_w \pi \rho_{air} l_a D_r^4 n_s^3 \tag{12}$$

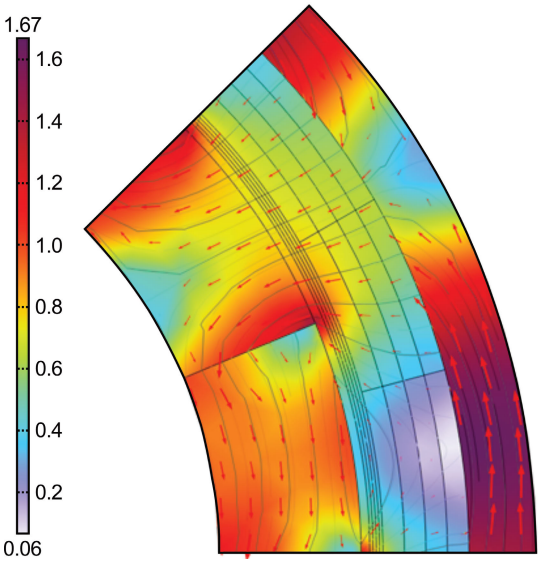

FIGURE 13. Mapping of the flux density distribution over one pole at rated operation of the 2.5-MW slotless generator in the FEA environment.

5) TOTAL EFFICIENCY

The overall generator efficiency is expressed in eq. (13).

$$\eta = \frac{P_e}{P_e + P_{cu} + P_{fe} + P_{pm} + P_w} \tag{13}$$

IV. RESULTS AND DISCUSSION

A thorough investigation of the new concept with the help of finite element analysis (FEA) was performed. Benchmarking of the new slotless PM design versus the existing high-speed generators for the same application has shown the advantages of the fiberprinted coreless PM technology in terms of compactness, low weight, and efficiency, as we will explore in this section.

A. SLOTLESS MACHINE CHARACTERIZATION

The flux density map of the slotless generator in Fig. 13 shows that the flux density in the south-orientated magnet's lower section and the west-orientated corners are significantly lower than in the rest of the magnets. Nevertheless, the machine is shown to be well magnetically utilized at full load. Initially, the same machine was designed analytically with slightly larger dimensions [25], as shown in Table 7. Some of the preliminary oversizing can be explained by the assumption of a larger airgap height, implying more magnets in the rotor.

The obtained terminal voltage for the maximum torque per ampere (MTPA) mode is shown in Fig. 14. It can be seen that the armature reaction is small, which is common for slotless machines. Even though the behavior of each segment is very similar, there are slight variations in inductance, as shown in Table 8. Segment 4 is closer to the stator yoke. Consequently, the phase inductances of segment 4 are 16.6 % larger than in segment 1. As a result, we see in Table 9 that segment 4 has a

TABLE 7. Comparison of FEA-optimized slotless generator against preliminary analytical design [25].

	FEA	Analytical	Deviation
D_r	275.0 mm	297.4 mm	+8.15 %
D_s	356.2 mm	411.4 mm	+15.50 %
l_a	238.0 mm	293.7 mm	+23.40 %
l_m	32.5 mm	39.0 mm	+20.00 %
δ	3.0 mm	4.8 mm	+60.00 %
h_s	4.9 mm	7.0 mm	+42.86 %
h_y	16.0 mm	26.1 mm	+63.13 %

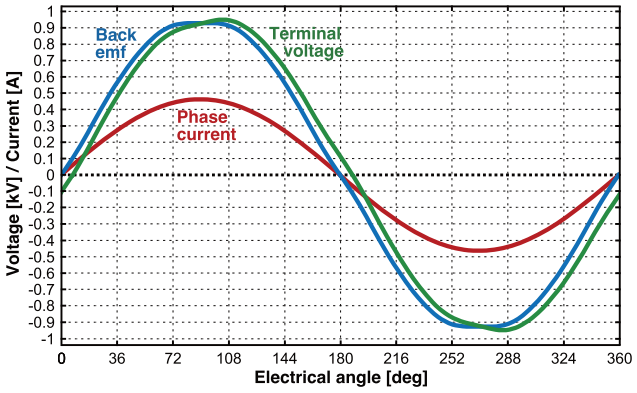

FIGURE 14. FEA-calculated no-load back-emf phase voltage and rated terminal phase voltage with sinusoidal nominal current loading obtained for inner armature segment (segment 1) for one phase of the 2.5-MW slotless generator.

TABLE 8. Direct-axis, quadrature-axis, and total phase inductance of each stator segment obtained in the FEA environment.

	L_d	L_q	$L_{ph} = \sqrt{L_d^2 + L_q^2}$
Segment 1	39.24 μH	50.88 μH	64.25 μH
Segment 2	43.12 μH	55.40 μH	70.20 μH
Segment 3	45.27 μH	58.42 μH	73.91 μH
Segment 4	45.27 μH	59.72 μH	74.94 μH
Mean	3.23 μH	56.11 μH	70.83 μH

TABLE 9. Rated terminal line voltages (rms) for each stator segment.

	Segment 1	Segment 2	Segment 3	Segment 4	Mean
U_l	1.172 kV	1.118 kV	1.085 kV	1.068 kV	1.111 kV

deeper armature reaction with a 8.9 % lower terminal voltage at rated load. The mean characteristics of the segments are provided in Table 10. We see that the normalized inductance is 0.228 pu per segment, which is a low value that is common for slotless machines. By utilizing the mean back emf for all four segments, provided in Table 10, the average torque can be estimated semi-analytically expressed in eq. (14). In Fig. 15, the semi-analytical torque match well with the stress-tensor-calculated torque in the FEA environment, providing an initial results validation.

$$\Gamma_e \approx N_s \frac{\sqrt{3} E_l I_{ph}}{2\pi n_s/60} \tag{14}$$

TABLE 10. Mean characteristics of each of the four armature segments obtained in the FEA environment.

P_e	E_l	U_l	I_{ph}	$\cos(\varphi)$	L_{ph}	R_{ph}
625.96 kW	1.10 kV	1.11 kV	328 A	0.9917	70.83 μH	4.25 mΩ

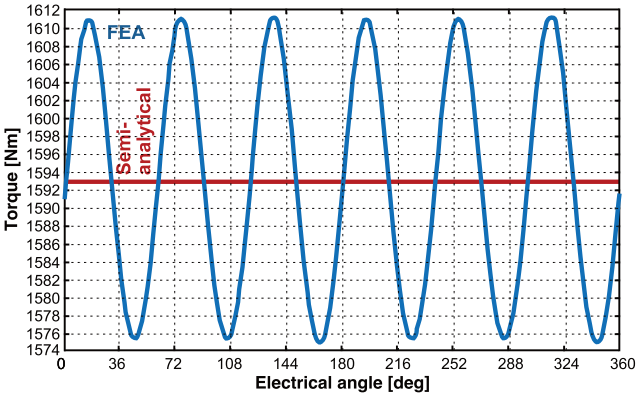

FIGURE 15. Rated time-dependent torque for the 2.5-MW slotless generator in the FEA environment. Comparison against the semi-analytical calculation in eq. (14) using the mean back-emf.

TABLE 11. Power densities with different rotor diameters from a parametric sweep in the FEA environment, using initial parameters.

Rotor diameter (D_r)		Active power density (ϱ_a)	
240.0 mm		24.83 kW/kg	
245.0 mm	(+2.08 %)	25.02 kW/kg	(+0.77 %)
250.0 mm	(+4.17 %)	25.14 kW/kg	(+1.25 %)
255.0 mm	(+6.25 %)	25.25 kW/kg	(+1.69 %)
260.0 mm	(+8.33 %)	25.37 kW/kg	(+2.17 %)
265.0 mm	(+10.42 %)	25.44 kW/kg	(+2.45 %)
270.0 mm	(+12.50 %)	25.46 kW/kg	(+2.54 %)
275.0 mm	(+14.58 %)	25.53 kW/kg	(+2.82 %)
280.0 mm	(+16.67 %)	25.53 kW/kg	(+2.82 %)

Power densities only considering active machine mass, excluding the mass of the end-windings.

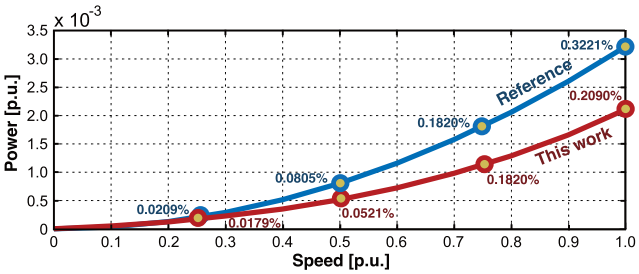

FIGURE 16. Comparison of speed-dependent no-load losses of the 2.5-MW slotless generator against the Mark 1, E-fan X generator [5], [6].

B. VERIFICATION OF POWER DENSITY OPTIMIZATION

The power densities of the slotless generator were optimized with a stator armature current density (rms) of 15 A/mm^2. We will go through some steps that were taken to reach the final design to provide confidence that the machine is indeed optimized well. In all the parametric sweeps, the flux density through the yoke was kept constant at 1.7 T by adjusting the

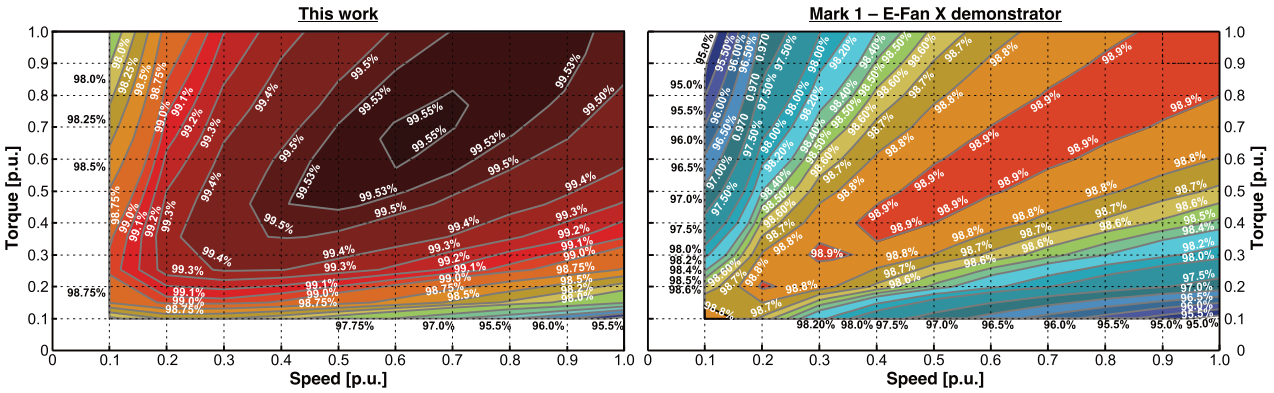

FIGURE 17. Efficiency (η) map comparison of the 2.5-MW slotless generator in percent, from this work, with sinusoidal armature current against the Mark 1, E-fan X generator [5], [6].

TABLE 12. Power densities with different magnet heights from a parametric sweep in the FEA environment, using initial parameters.

Magnet height (l_m)		Active power density (ϱ_a)	
20.0 mm		24.43 kW/kg	
22.5 mm	(+12.50 %)	24.91 kW/kg	(+1.96 %)
25.0 mm	(+25.00 %)	25.18 kW/kg	(+3.07 %)
27.5 mm	(+37.50 %)	25.38 kW/kg	(+3.89 %)
30.0 mm	(+50.00 %)	25.47 kW/kg	(+4.23 %)
32.5 mm	(+62.50 %)	25.54 kW/kg	(+4.54 %)
35.0 mm	(+75.00 %)	25.53 kW/kg	(+4.50 %)

Power densities only considering active machine mass, excluding the mass of the end-windings.

TABLE 13. Suboptimized and final optimized active weight power densities of the slotless generator, Excl. and Incl. End-winding mass.

		ϱ_a
Suboptimized	Rotor diameter (D_r)	25.53 kW/kg
	Magnet height (l_m)	25.54 kW/kg
Final optimized	Excl. end-winding mass	26.95 kW/kg
	Incl. end-winding mass	24.38 kW/kg

TABLE 14. Mass distribution of the 2.5-MW slotless generator.

Part	Material	Symbol	Mass	Mass fraction
Permanent magnet	NdFeB (N50)	m_{pm}	44.96 kg	43.8 %
Rotor enclosure	Carbon sleeve	m_{enc}	0.73 kg	0.70 %
Armature winding	Copper	m_{cu}	14.07 kg	13.7 %
End-winding	Copper	m_{ew}	9.79 kg	9.6 %
Winding insulation	Nomex 993	m_{ins}	3.79 kg	3.7 %
Stator yoke	10JNEX900	m_{fe}	29.20 kg	28.5 %
Total active mass		m_a	102.54 kg	100 %

yoke height. In addition, the current loading of the machine was adjusted to comply with approximately 1.59 kNm at 15 000 rpm, yielding an electrical power of approximately 2.5 MW.

1) OPTIMAL ROTOR DIAMETER (D_r)

A parametric sweep of the slotless generator's power density as a function of rotor diameter is presented in Table 11, with 240 mm as the starting point. The rotor diameter was incrementally increased to reach maximum power density. Table 11 highlights that a rotor diameter of 275 mm was selected and preferred over a rotor diameter of 280 mm.

2) OPTIMAL MAGNET HEIGHT (l_m)

Similarly, the slotless generator's power densities with different magnet heights are listed in Table 12. The highest power density is achieved with a magnet height of 32.5 mm. In relative terms, the difference in performance from the worst to best magnet height was 4.54 %.

3) FINAL POWER DENSITY

After the optimal rotor diameter and magnet height were both settled, their combination only triggered minor adjustments to ensure that the stator yoke achieved a mean yoke flux density of about 1.7 T. The effects of both these optimizations resulted in an even higher power density than achieved independently, as seen in Table 13, which also takes into account the power density, including the end-winding. The overall mass distribution for the optimized machine is provided in Table 14.

C. COMPARISON AGAINST THE-STATE-OF-THE-ART

Two competitive prototypes, developed for the aero generator application and based on conventional iron-cored PM technology, were chosen as benchmarks. These prototypes were presented by Golovanov et al. [3] and Wang et al. [4]. A comparison of these prototypes with the slotless PM technology based on FiberPrinting^{TM}, as depicted in Table 15, reveals clear advantages of the new technology. It achieves a power density of over 24 kW/kg, competitive with the performance of the benchmarks, while ensuring an ultra-high efficiency beyond 99 %. These combined performance characteristics have been unattainable with conventional iron-cored technologies due to higher losses and the iron-core saturation problem. The research findings indicate that the proposed

TABLE 15. Comparison of figures of merit for the high-speed MW-class generators (2.5 MW and 3.6 MW) against the state-of-the-art (SotA).

		SotA		This work	
Parameter	Symbol	Golovanov et. al. (2021) [3]	Wang et. al. (2023) [4]	Original design	Revised design(*)
Rated electrical power	P_e	4.0 MW	1.0 MW	2.5 MW	3.6 MW
Nominal rotational speed	n_s	15 000 rpm	20 000 rpm	15 000 rpm	15 000 rpm
Electrical torque	Γ_e	2548 Nm	478 Nm	1592 Nm	2292 Nm
Power factor	$\cos(\varphi)$	0.820	0.708	0.992	0.991
DC bus voltage	U_{dc}	3000 V	2000 V	3000 V	3000 V
Number of poles	p	8	12	8	12
Electrical frequency	f	1000 Hz	2000 Hz	1000 Hz	1500 Hz
Number of phases	$N_s \times N_{ph}$	8×3	6×3	4×3	4×3
Phase voltage (rms)	$U_l/\sqrt{3}$	491.0 V	271.1 V	640.3 V	922.9 V
Phase current (rms)	I_{ph}	414.0 A	289.4 A	328.0 A	328.0 A
Stator current density (rms)	J_s	27.5 A/mm^2	20.0 A/mm^2	15.0 A/mm^2	27.5 A/mm^2
Rated efficiency	η_n	98.3 %	97.3 %	99.4 %	98.5 %
Active power density(**)	ϱ_a	35.4 kW/kg	23.7 kW/kg	24.4 kW/kg	42.6 kW/kg
Total power density	ϱ_{tot}	17.3 kW/kg	9.0 kW/kg	12.2 kW/kg	21.3 kW/kg
Active torque density(**)	τ_a	22.5 Nm/kg	11.3 Nm/kg	15.5 Nm/kg	27.1 Nm/kg
Total torque density	τ_{tot}	11.0 Nm/kg	4.3 Nm/kg	7.8 Nm/kg	13.6 Nm/kg

(*) The stator armature winding is 45 % smaller, and the stator yoke is reduced by 40 %.
(**) Active power and torque densities only consider active machine mass.

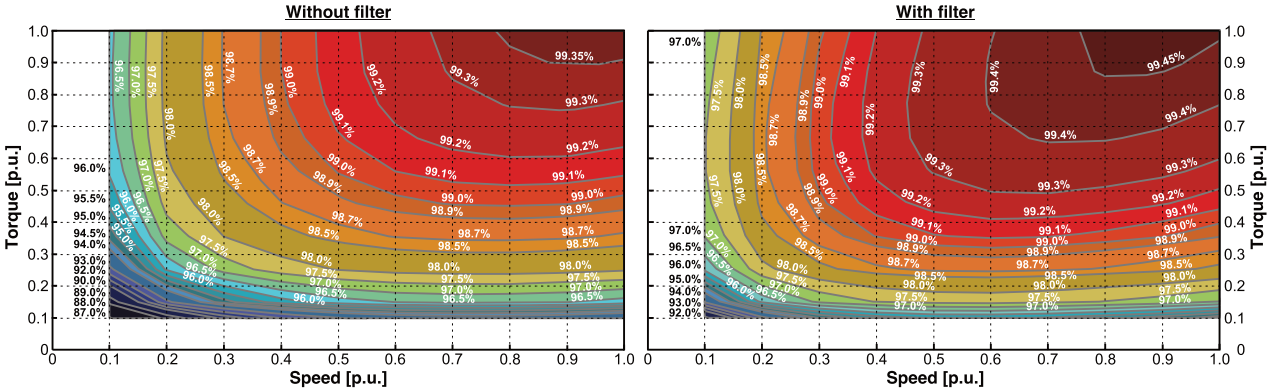

FIGURE 18. Efficiency (η) map comparison of the 2.5-MW slotless generator in percent, from this work, with inverter-fed armature current, with and without filter. Calculations based on analytical switching model presented in Fig. 19.

technology enables the development of a lightweight machine with cooling requirements reduced by two to three times compared to the reference machines. In addition, Table 15 also reports a revised design where the number of poles was increased from 8 to 12, and the current density was enhanced from 15 A/mm^2 to 27.5 A/mm^2, similar to Golovanov et al. [3]. Even though the efficiency was greatly reduced to below 99 %, the power density was enhanced to nearly 43 kW/kg. Increased number of poles significantly reduced the mass of the stator yoke, while the ultra-high current density also reduced the mass of the stator armature. As a result, both the original and the revised designs show great potential to exceed the state-of-the-art (SotA) both in terms of efficiency and power density.

To provide another insightful comparison, a detailed benchmarking was done against Rolls-Royce's 2.5 MW, 3 kV, 15 000 rpm generator [5], [6]. In Fig. 16, it is shown that this work achieves a 35 % reduction in the speed-dependent no-load losses. Fig. 17 shows that the proposed slotless

TABLE 16. Rated loss distribution in the 2.5-MW slotless generator, without ripple (Sinusoidal excitation) and with ripple (Filtered).

		Without ripple		With ripple (filtered)	
Part	Symbol	Loss component	Loss fraction	Loss component	Loss fraction
Magnet	P_{pm}	0.130 kW	1.07 %	3.845 kW	23.67 %
Copper	P_{cu}	6.748 kW	55.71 %	6.819 kW	41.99 %
Iron	P_{fe}	1.930 kW	15.93 %	2.271 kW	13.99 %
Windage	P_w	3.305 kW	27.29 %	3.305 kW	20.35 %
Total	P_{loss}	12.113 kW	100 %	16.240 kW	100 %

generator has a nominal efficiency of 99.5 %, while the reference (Mark 1, E-Fan X) has a peak efficiency of 98.9 %. Higher efficiency in the rated operation area corresponds to about 55 % lower losses. As a result, 55 % less heat must be removed, and the cooling system can be smaller and lighter.

Fig. 17 considers only the ideal sinusoidal excitation of the machines. Therefore, a secondary investigation was done to

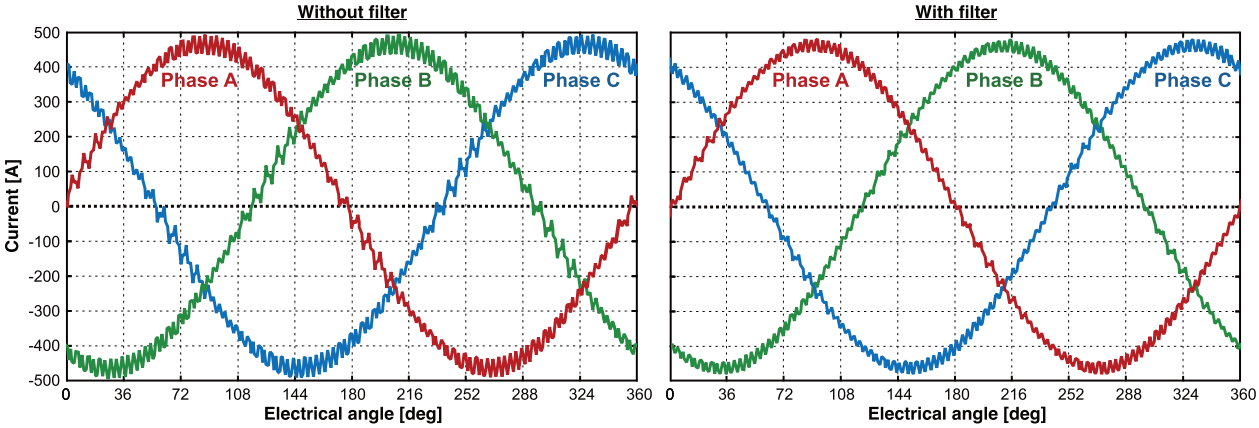

FIGURE 19. Phase currents injected into segment 1 in the FEA environment with and without additional filter. Waveforms obtained from an existing analytical algorithm in Matlab [26], [27]. Switching frequency (f_{sw}) is set equal to 50 kHz. Filter model has an inductance of 50 uH per stator segment [29], [30]. A similar analysis was done for the other segments as well.

TABLE 17. 2.5-MW hybrid-electric generator system performance with filter (Excl. Circuit breakers and thermal management).

Component	Component mass	Total power density	Power input	Power output	Component efficiency	Sources
1x Generator (2.5 MW)	205.08 kg	12.19 kW/kg	2.51 MW	2.50 MW	99.44 %	This work
4x Filters	139.84 kg	17.86 kW/kg	2.50 MW	2.50 MW	99.90 %	[29], [30]
4x Inverters	123.63 kg	20.00 kW/kg	2.50 MW	2.47 MW	99.00 %	[31], [32]
1x 20 m DC cable (3 kV)	88.74 kg	27.78 kW/kg	2.47 MW	2.47 MW	99.70 %	[32], [33]
Overall	557.29 kg	4.42 kW/kg	2.51 MW	2.47 MW	98.05 %	[29]–[33]

TABLE 18. 2.5-MW hybrid-electric generator system performance without filter (Excl. Circuit breakers and thermal management are excluded).

Component	Component mass	Total power density	Power input	Power output	Component efficiency	Sources
1x Generator (2.5 MW)	205.08 kg	12.19 kW/kg	2.52 MW	2.50 MW	99.35 %	This work
4x Inverters	123.75 kg	20.00 kW/kg	2.50 MW	2.48 MW	99.00 %	[31], [32]
1x 20 m DC cable (3 kV)	88.83 kg	27.78 kW/kg	2.48 MW	2.47 MW	99.70 %	[32], [33]
Overall	427.66 kg	5.77 kW/kg	2.52 MW	2.47 MW	98.06 %	[31]–[33]

obtain the efficiency map for the original design considering inverter-fed excitation. Fig. 18 highlights that the efficiency reduces to 99.44 % at rated conditions without filters. However, including a filter, the nominal efficiency can reach 99.35 %, where the loss distribution is shown in Table 16. The reduced ripple in the phase currents obtained using filters is shown in Fig. 19, which was based on an existing analytical algorithm to create realistic current waveforms to feed into the FEA environment [26], [27].

D. OVERALL PERFORMANCE OF GENERATOR SYSTEM

In the overall system performance evaluation, the electric propulsion motor located on the wing is not included. Only the hybrid-electric generator system is considered. Tables 17 and 18 compare the system performance with and without filters. Even though the filter improves the efficiency of the generator, the overall efficiency remains the same. Nevertheless, the power density is superior when excluding the filter. Moreover, the thermal management system needed to cool the generator could add about 20 kg in extra mass [28]. In the study, it was assumed that the cooling would be arranged through the spaces between the concentric rings, thus providing direct liquid cooling of the hottest parts of the machine. However, the exact solution remains to be derived in future research.

V. CONCLUSION

This paper presents the figures of merit of a 3-kV, 2.5-MW, 15000-rpm, slotless generator for a hybrid-electric aircraft application. We show that it can achieve a power density of 24.38 kW/kg when the active mass is considered, including the end-winding. The system-level performance was evaluated for two cases, with and without inverter-fed current harmonics, which resulted in efficiencies of 99.35 % and 99.44 %, respectively. The main impact from the inverter was found in a thirty-fold increase in the magnet losses (including filter), yielding a reduction in overall efficiency. Nevertheless, the steel losses were kept low using the electrical steel 10JNEX900, suited for high-frequency operation.

In the end, another revised design was explored to identify the impact of elevating the current density to levels comparable to the state-of-the-art (SotA) reference machines (20-27.5 A/mm^2). Our results indicate that such an enhancement would significantly raise the power density to 35-40 kW/kg. Furthermore, increasing the number of poles from 8 to 12, in combination with the elevated current density, can help the slotless machine surpass the threshold of 40 kW/kg and significantly exceed the SotA power densities.

The efficiency of the 3-kV, 2.5-MW slotless generator was also compared to the Mark 1 generator from the E-fan X project. The slotless generator has a superior performance, achieving lower losses at full-load and no-load conditions. Moreover, the efficiency of the hybrid-electric generator system was slightly above 98 % with and without the filter. However, the filter adds 140 kg to the total system mass, reducing the overall power density of the system from 5.77 kW/kg to 4.42 kW/kg. Therefore, a system without a filter is preferred unless the rotor temperature must be reduced. Then a filter will reduce the magnet losses and the rotor temperature.

In summary, the concept of four galvanically isolated concentric rings shows promising results regarding efficiency and power density, while the concept itself could provide improved reliability. System fault tolerance and cooling needs could be further explored to assess its potential role in realizing hybrid-electric aviation.

ACKNOWLEDGMENT

The authors would like to thank Yannick Cyiza Karekezi and Runar Mellerud for their help with setting up simulations and conducting analysis in the FEA environment.

REFERENCES

[1] P. Wheeler, T. S. Sirimanna, S. Bozhko, and K. S. Haran, "Electric/hybrid-electric aircraft propulsion systems," *Proc. IEEE*, vol. 109, no. 6, pp. 1115–1127, Jun. 2021.

[2] G. E. Wroblewski and P. J. Ansell, "Hybrid-electric regional jet aircraft operation efficiency," in *Proc. AIAA/IEEE Electr. Aircr. Technol. Symp. (EATS)*, Aug. 2019, pp. 1–22.

[3] D. Golovanov, D. Gerada, G. Sala, M. Degano, A. Trentin, P. H. Connor, Z. Xu, A. L. Rocca, A. Galassini, L. Tarisciotti, C. N. Eastwick, S. J. Pickering, P. Wheeler, J. Clare, M. Filipenko, and C. Gerada, "4-MW class high-power-density generator for future hybrid-electric aircraft," *IEEE Trans. Transport. Electrific.*, vol. 7, no. 4, pp. 2952–2964, Dec. 2021.

[4] J. Wang, T. Jahns, P. McCluskey, J. Kizito, B. Sarlioglu, R. Borjas, J. Swanke, Y. Cong, Z. Yao, H. Zeng, P. Fu, and A. Schnabel, "2-kV 1-MW 20,000-RPM integrated modular motor drive for electrified aircraft propulsion," *IEEE J. Emerg. Sel. Topics Power Electron.*, early access, Jun. 7, 2023, doi: 10.1109/JESTPE.2023.3283538.

[5] J. K. Nøland, M. Leandro, J. A. Suul, and M. Molinas, "High-power machines and starter-generator topologies for more electric aircraft: A technology outlook," *IEEE Access*, vol. 8, pp. 130104–130123, 2020.

[6] S. Øvrebø, S. Tiwari, and S. Skaar, "Test and validation of the mark 1 (2.5 MW) E-fan X generator," in *Proc. NATO AVT-RSY-Res. Symp. Hybrid/Electr. Aero-Propuls. Syst. Military Appl.*, Oct. 2019, pp. 1–9, Paper NBR 19.

[7] A. Yoon, X. Yi, J. Martin, Y. Chen, and K. Haran, "A high-speed, high-frequency, air-core PM machine for aircraft application," in *Proc. IEEE Power Energy Conf. Illinois (PECI)*, Feb. 2016, pp. 1–4.

[8] M. S. Islam, R. Mikail, and I. Husain, "Slotless lightweight motor for aerial applications," *IEEE Trans. Ind. Appl.*, vol. 55, no. 6, pp. 5789–5799, Nov. 2019.

[9] S. Collins, P. Mellor, and N. Simpson, "Experimental investigation of a slotless skewed stator with a composite winding layer," in *Proc. IEEE Energy Convers. Congr. Expo. (ECCE)*, Oct. 2021, pp. 3659–3666.

[10] M. Sanada and S. Morimoto, "Efficiency improvement in high speed operation using slot-less configuration for permanent magnet synchronous motor," in *Proc. IEEE Power Eng. Soc. Gen. Meeting*, Jun. 2007, pp. 1–7.

[11] N. Dave, G. Vakil, Z. Xu, C. Gerada, H. Zhang, and D. Gerada, "Comparison of slotted and slotless PM machines for high kW/kg aerospace applications," in *Proc. 23rd Int. Conf. Electr. Mach. Syst. (ICEMS)*, Nov. 2020, pp. 609–613.

[12] D. Lee, T. Balachandran, N. Salk, J. Schuh, A. Yoon, P. Xiao, Y. Yu, S. Lin, P. Powell, and K. K. Haran, "Design and prototype of a high power density slotless PMSM for direct drive aircraft propulsion," in *Proc. IEEE Power Energy Conf. Illinois (PECI)*, Apr. 2021, pp. 1–6.

[13] A. D. Anderson, Y. Wang, Y. Yu, and K. S. Haran, "Experimental validation of a high-power slotless stator," in *Proc. IEEE Int. Electr. Mach. Drives Conf. (IEMDC)*, May 2019, pp. 1564–1569.

[14] A. Matveev, "Energy conversion system," NO Patent 345 844 B1, Aug. 30, 2021.

[15] H. Zeng, J. Swanke, T. M. Jahns, and B. Sarlioglu, "Modular modeling and distributed control of permanent-magnet modular motor drives (MMDs) for electric aircraft propulsion," in *Proc. IEEE Energy Convers. Congr. Expo. (ECCE)*, Oct. 2021, pp. 4598–4605.

[16] E. K. Mikkelsen, "Design and analysis of a 2.5 MW coreless aero generator for hybrid-electric aircraft," M.S. thesis, Dept. Electr. Energy, Norwegian Univ. Sci. Technol. (NTNU), Trondheim, Norway, Jun. 2023.

[17] J. Selnes, "Electromagnetic mat for a stator or rotor component of an electric machine," EP Patent 3 695 488 B1, Nov. 10, 2021.

[18] Z. Song, C. Liu, K. Feng, H. Zhao, and J. Yu, "Field prediction and validation of a slotless segmented-Halbach permanent magnet synchronous machine for more electric aircraft," *IEEE Trans. Transport. Electrific.*, vol. 6, no. 4, pp. 1577–1591, Dec. 2020.

[19] C. Deak, L. Petrovic, A. Binder, M. Mirzaei, D. Irimie, and B. Funieru, "Calculation of eddy current losses in permanent magnets of synchronous machines," in *Proc. Int. Symp. Power Electron. Electr. Drives Autom. Motion*, 2008, pp. 26–31.

[20] A. Hebala, S. Nuzzo, P. H. Connor, P. Giangrande, C. Gerada, and M. Galea, "PM Halbach arrays in motors: Loss reduction and performance improvements," in *Proc. 23rd Int. Conf. Electr. Mach. Syst. (ICEMS)*, Nov. 2020, pp. 710–715.

[21] D. M. Ionel, M. Popescu, M. I. McGilp, T. J. E. Miller, S. J. Dellinger, and R. J. Heideman, "Computation of core losses in electrical machines using improved models for laminated steel," *IEEE Trans. Ind. Appl.*, vol. 43, no. 6, pp. 1554–1564, Nov. 2007.

[22] A. Al-Timimy, P. Giangrande, M. Degano, M. Galea, and C. Gerada, "Investigation of AC copper and iron losses in high-speed high-power density PMSM," in *Proc. 13th Int. Conf. Electr. Mach. (ICEM)*, Sep. 2018, pp. 263–269.

[23] A. Bardalai, X. Zhang, T. Zou, D. Gerada, J. Li, and C. Gerada, "Comparative analysis of AC losses with round magnet wire and litz wire winding of a high—Speed PM machine," in *Proc. 22nd Int. Conf. Electr. Mach. Syst. (ICEMS)*, Aug. 2019, pp. 1–5.

[24] A. B. Nachouane, A. Abdelli, G. Friedrich, and S. Vivier, "Estimation of windage losses inside very narrow air gaps of high speed electrical machines without an internal ventilation using CFD methods," in *Proc. 22nd Int. Conf. Electr. Mach. (ICEM)*, Sep. 2016, pp. 2704–2710.

[25] E. K. Mikkelsen, "High-speed multi-megawatt-class aero generator for hybrid-electric airplanes," Dept. Electr. Energy, Norwegian Univ. Sci. Technol. (NTNU), Trondheim, Norway, Project Rep. TET4510, Dec. 2022.

[26] M. Leandro, "Induced PM eddy current model in slotless PM machines," Code Occean, Dept. Electr. Energy, Norwegian Univ. Sci. Technol. (NTNU), Trondheim, Norway, Tech. Rep., 2022, doi: 10.24433/CO.6124316.v2.

[27] M. Leandro and J. K. Nøland, "Analytical PM eddy currents loss evaluations in inverter-fed slotless machines induced by SVM control using polar coordinates formulations," *IEEE Trans. Energy Convers.*, early access, Jul. 12, 2023, doi: 10.1109/TEC.2023.3294807.

[28] J. M. Rheaume, M. Macdonald, and C. E. Lents, "Commercial hybrid electric aircraft thermal management system design, simulation, and operation improvements," in *Proc. AIAA/IEEE Electr. Aircr. Technol. Symp. (EATS)*, Aug. 2019, pp. 1–23.

[29] Y. Liu, K.-Y. See, S. Yin, R. Simanjorang, C. F. Tong, A. Nawawi, and J. J. Lai, "LCL filter design of a 50-kW 60-kHz SiC inverter with size and thermal considerations for aerospace applications," *IEEE Trans. Ind. Electron.*, vol. 64, no. 10, pp. 8321–8333, Oct. 2017.

[30] T. Appel, J. Fuhrmann, and H.-G. Eckel, "Design of inductive components for triangular current mode (TCM) inverters up to 500 kW," in *Proc. Int. Exhib. Conf. Power Electron. Intell. Motion Renewable Energy Manage.*, 2017, pp. 1–7.

[31] D. Wang, L. Zhou, P. Zheng, Y. Yang, A. Callegaro, P. Suntharalingam, M. Goykhman, A. Baronian, and A. Emadi, "1.5 kV, 1 MVA inverters for electric aircraft applications: A mission profile-based comparative study," in *Proc. IEEE Energy Convers. Congr. Expo. (ECCE)*, Oct. 2022, pp. 01–05.

[32] M. Filipenko, S. Biser, M. Boll, M. Corduan, M. Noe, and P. Rostek, "Comparative analysis and optimization of technical and weight parameters of turbo-electric propulsion systems," *Aerospace*, vol. 7, no. 8, p. 107, Jul. 2020.
[33] A. Azizi, M. Ghassemi, and J. Lehr, "Design of a cable system for a high-power density MVDC aircraft electric power system," in *Proc. IEEE Conf. Electr. Insul. Dielectr. Phenomena (CEIDP)*, Oct. 2022, pp. 151–154.

EIRIK KVÅLE MIKKELSEN was born in Bergen, Norway, in 1998. He received the M.Sc. degree in energy and environmental engineering from the Norwegian University of Science and Technology (NTNU), in 2023. His current research interests include electrical machines for aircraft applications and electrical machines in general.

ALEXEY MATVEEV received the M.Sc. degree in electrical engineering from the Moscow Power Engineering Institute, Russia, in 1998, and the Ph.D. degree in electrical engineering from the Eindhoven University of Technology, The Netherlands, in 2006. Since 1996, he has been working in a number of companies, including ABB, Vacon (now Danfoss), SmartMotor, Rolls-Royce, and Kongsberg Group. In 2019, he became the Research and IP Director of Alva Industries AS, Trondheim, Norway, and since 2022, he has been having a part-time position as an Adjunct Professor with the Norwegian University of Science and Technology (NTNU). His current research interests include the philosophy of technology, the evolution of electric machines, the application of TRIZ in electrical engineering, and the new configurations of electric machines and propulsion systems.

JONAS KRISTIANSEN NØLAND (Senior Member, IEEE) was born in Drammen, Norway, in 1988. He received the M.Sc. degree in electric power engineering from the Chalmers University of Technology, Gothenburg, Sweden, in 2013, and the Ph.D. degree in engineering physics from Uppsala University, Uppsala, Sweden, in 2017. He is currently an Associate Professor with the Department of Electric Power Energy, Norwegian University of Science and Technology (NTNU).

His current research interests include the improved utilization of electrical machines, high-power machinery for aircraft applications, and transportation electrification in general.

Dr. Nøland is the Chair of the IEEE Power and Energy Chapter of Norway. He also serves as an Associate Editor for the IEEE TRANSACTIONS ON ENERGY CONVERSION, the IEEE TRANSACTIONS ON INDUSTRIAL ELECTRONICS, and the IEEE TRANSACTIONS ON TRANSPORTATION ELECTRIFICATION.